Corrosion Science 80 (2014) 350–358

Contents lists available at ScienceDirect

Corrosion Science

journal homepage: www.elsevier.com/locate/corsci

Stress corrosion cracking under low stress: Continuous or discontinuous cracks?

Longkui K. Zhu [a], Yu Yan [a], Jinxu X. Li [a], Lijie J. Qiao [a,*], Alex A. Volinsky [b,a]

[a] Corrosion and Protection Center, Key Laboratory for Environmental Fracture (MOE), University of Science and Technology Beijing, Beijing 100083, People's Republic of China
[b] Department of Mechanical Engineering, University of South Florida, Tampa, FL 33620, USA

ARTICLE INFO

Article history:
Received 28 June 2013
Accepted 29 November 2013
Available online 5 December 2013

Keywords:
A. Stainless steel
B. SEM
B. Modelling studies
C. Stress corrosion
C. Anodic dissolution

ABSTRACT

Two-dimensional and three-dimensional crack morphologies of stress corrosion cracking (SCC) were studied by serial-sectioning and synchrotron-based X-ray computed tomography. Discontinuous surface cracks were actually continuous inside the specimen, which matched typical river-like fractographs and finite element simulations. A low stress SCC model was created, where a main crack continuously grew along the main propagation direction (MPD) due to anodic dissolution; then, discontinuous secondary microcracks emanated from MPD, angularly extending to the two sides of MPD. Finally, some of the secondary microcracks reached the sample surface, resulting in the formation of discontinuous surface cracks.

1. Introduction

Transgranular stress corrosion cracking (TGSCC) is a typical fracture mode for the SCC system of stainless steels in chloride environments, characterized by river-like fractographs [1–5]. It has been reported that the environmental fracture is discontinuous at the micron scale [4]. Recently, two-dimensional (2-D) detection of TGSCC has indicated that surface cracks in fact nucleate discontinuously and then can connect with each other through breaking of the ligaments between the main crack and the microcracks, especially at the low stress levels [6–8]. In order to elucidate the controlling electrochemical/physical mechanism of the cleavage-like fracture, a corrosion-enhanced plasticity model (CEPM) has been proposed. In CEPM the local stresses increase due to dislocation pile-ups, while the critical stress intensity factor, K_{IC}, decreases due to hydrogen, leading to the microcracks initiation in front of the main crack tips, which finally results in the formation of the river-like fractographs [2–4,9,10]. The 2-D discontinuity of the TGSCC propagation is experimentally and theoretically proven to be reasonable. However, TGSCC is a three-dimensional (3-D) process. To understand the mechanism and more accurately predict the crack growth, it is essential to examine inner geometrical features of discontinuous surface TGSCC cracks.

Inside the specimen, it is a critical issue whether the fracture process is continuous or discontinuous. In theory, apart from the discontinuity, suggested by CEPM, it is also possible for microcracks to initiate continuously when the crack propagation is controlled by anodic dissolution (AD). Numerous experimental results have shown that SCC under low stress should be attributed to an AD mechanism. For example, anodic polarization accelerated SCC [11–13]. The normalized threshold stress intensity factor of SCC, K_I/K_{ISCC}, was much lower than that of hydrogen induced cracking, K_I/K_{IH} [14,15], and most SCC cracks originated from the pits [16–19]. The slip-dissolution model, sometimes called the film-rupture model, has been developed and is referred to as a relatively mature and successful attempt to rationalize the kinetics of SCC [20]. It postulates that either emerging slip planes or simply exposing fresh metal surfaces by rupturing protective films act as anodes. This speeds up metal dissolution prior to re-appearance of the planes, or re-establishment of protective films, while repetition of this sequence makes the cracks longer [20–26]. Hall [25,26] further pointed out that SCC was active path corrosion, assisted by yielding or film rupture. From this perspective, there should be an existing AD path, and TGSCC is continuous inside the samples, which is completely different from the CEPM predictions. Therefore, the inner SCC cracks continuity or discontinuity determines the primary fracture mechanism.

Several researchers have recently addressed 3-D SCC cracks. Marrow et al. [27–29] systematically studied intergranular SCC of a sensitized austenitic stainless steel by means of 2-D fractography and 3-D X-ray computed tomographic images. They found that the discontinuous surface crack was actually continuous within the specimen. However, few experimental efforts have addressed

* Corresponding author. Address: Corrosion and Protection Center, Key Laboratory for Environmental Fracture (MOE), University of Science and Technology Beijing, Beijing 100083, People's Republic of China. Tel.: +86 10 6233 4499; fax: +86 10 6233 2345.
E-mail addresses: lqiao@ustb.edu.cn (L.J. Qiao), volinsky@usf.edu (A.A. Volinsky).

0010-938X/$ - see front matter © 2013 Elsevier Ltd. All rights reserved.
http://dx.doi.org/10.1016/j.corsci.2013.11.057

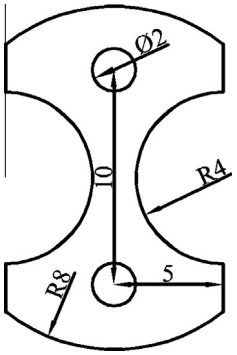

Fig. 1. Schematics of 316L stainless steel single crystal specimens (dimensions in mm).

how the inner TGSCC cracks advance and how the surface discontinuous cracks form. This work aims to detect the continuity or discontinuity of crack propagation paths inside the specimens and attempts to construct a model of TGSCC. In general, approaches to inner crack morphology characterization can be grouped into two categories: destructive serial-sectioning [23,30] and nondestructive X-ray computed tomography [27–29]. The former offers high-resolution slices, while the latter presents the benefits of in situ 3-D visualization of cracks. In this work, both methods have been used to illustrate the TGSCC propagation.

2. Experimental procedure

2.1. SCC test

316L SS single crystals were used in this study with the following chemical composition: C-0.007 wt.%, Cr-17.00 wt.%, Ni-13.49 wt.%, Mo-2.54 wt.%, Mn-0.66 wt.%, Si-0.46 wt.%, P-0.0080 wt.%, S-0.0056 wt.%, Fe-balance. The crystals were produced along [0 0 1] direction and machined into 0.7 mm thick specimens with 2 mm circular holes. Prior to the experiments, the specimens were annealed at 1050 °C for 30 min in argon, water-quenched, followed by grinding to 2000 grit, and were electrochemically thinned to about 0.5 mm in solutions containing H_3PO_4, H_2SO_4, CrO_3 and glycol ($C_2H_6O_2$). Finally, the samples were degreased with acetone in an ultrasonic cleaner and washed with deionized water. The specimen geometry is shown in Fig. 1. After the pretreatment, the samples were placed into a glass container filled with a boiling 45 wt.% $MgCl_2$ solution. A low nominal stress of 20 MPa, calculated according to the narrowest section (2×0.5 mm^2), was applied to the specimen. All experiments were carried out under an open circuit condition, using a weight-type constant load apparatus equipped with a cooling system, two 316L SS single crystal rods and two silica grips. After testing, each specimen was ultrasonically cleaned in deionized water as well as a 5 wt.% HCl + 2 g L^{-1} hexamethylenetetramine mixture, and then TGSCC cracks and fractographs were observed by scanning electron microscopy (SEM) and optical microscopy.

2.2. Approaches to inner crack morphology characterization

Both destructive serial-sectioning and nondestructive X-ray computed tomography were utilized to directly observe the inner discontinuous surface cracks. First, surface layers of the specimens were removed via mechanical polishing and the cracks were observed in SEM. In this way, a series of 2-D cracks at different distance beneath the specimen top surface were obtained and compared to determine whether the cracks were continuous or not. Second, the X-ray computed tomography was used to directly visualize 3-D morphologies of discontinuous surface cracks. To perform tomographic imaging, samples with cracks (about 0.5×0.5 mm^2 cross-sections) were prepared by the following method: wire-electrode cutting; rinsing in acetone; cleaning in deionized water; hot air drying and storing in a desiccated chamber. Subsequently, the computed tomographic experiments were conducted using the BL13W1 beam line at the Shanghai Synchrotron Radiation Facility (SSRF). Almost monochromatic X-ray beam was used with the energy of 42 keV, and a high-speed camera recorded transmitted intensity in an 8 s exposure/projection interval, while the sample was rotated in 0.25° increments. During each 180° rotation, 720 2-D radiographs were recorded and applied to the reconstruction of image slices nearly perpendicular to the crack growth direction. Isotropic voxels with the resolution of 0.7 μm were achieved in the reconstructed slices. Next, image analysis, visualization and 3-D rendering were carried out using a commercial software package (Amira). The whole X-ray computed tomographic process is illustrated in Fig. 2. Additionally, the fractograph was also detected to verify the 3-D crack morphology along with the continuity or the discontinuity of the cracks.

2.3. Finite element analysis

ABAQUS V6.10-1 was used to simulate the stress and strain distribution near the fronts of 3-D crack tips with and without a defect. To simplify the calculation, a 3-D equivalent rectangular specimen was modeled with the dimensions of $2 \times 10 \times 0.5$ mm^3, and a 0.3×0.1 mm^2 semi-elliptic through crack (the half length of the axis in the direction "1" × the half length of the axis in the direction "2") was created at the center of the specimen length in the direction "2", shown in Fig. 3. Due to geometric symmetry, a half of the model was used, shown in Fig. 3(a). Then, an initial defect was cut at the crack front of the pre-cracked specimen. The shape of the initial defect was obtained by rotating a 0.06×0.04 mm^2 semi-ellipse (the half length of the axis in the direction "1" × the half length of the axis in the direction "3" (the thickness direction)) about the crack front, as shown in Fig. 3(c). In this model, the half length of the defect axis in the direction "3" was changed from 0.04 mm to 0.14 mm in order to investigate the effect of the defect size on the stress and strain distribution. For the models with and without the defect, the mesh was created using the 3-D elements C3D20, which are quadratic 20-node elements. The boundary conditions were as follows:

$$\begin{aligned} y = 5, \quad u_y = 0.0005 \\ y = 0, \quad u_y = 0 \end{aligned} \tag{1}$$

The Young modulus of 188 GPa and Poisson's ratio of 0.3 for 316L SS single crystal were the input parameters for the FE model. The normal stress, S_{22}, and the normal strain, LE_{22}, along the tensile direction were used in the analysis to characterize the mechanical behavior of this material.

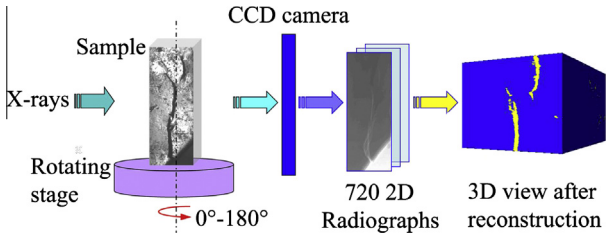

Fig. 2. Schematic diagram of the whole X-ray computed tomographic process.